Korean J. Chem. Eng., 32(12), 2369-2374 (2015)
DOI: 10.1007/s11814-015-0222-8

pISSN: 0256-1115
eISSN: 1975-7220

RAPID COMMUNICATION

Synthesis and thermodynamic properties of a novel pyridinium-based asymmetrical gemini ionic liquid

Xuzhao Yang†, Jun Wang†, Wenyuan Zou, and Jinchao Wu

Henan Provincial Key Laboratory of Surface and Interface Science,
Collaborative Innovation Center of Environmental Pollution Control and Ecological Restoration,
Zhengzhou University of Light Industry, Zhengzhou 450002, P. R. China
(*Received 26 August 2015 • accepted 18 October 2015*)

Abstract−A novel asymmetrical gemini ionic liquid (GIL), [1-(1-pyridinium-yl-hexyl)-6-methylpiperidinium] dihexafluorophosphate ($[PyC_6MPi][PF_6]_2$) combined with pyridine, 1-methylpiperidine by 1,6-dibromohexane with PF_6^- as anion, was synthesized and characterized by ^1H NMR and IR. The molar heat capacity of the GIL was measured via differential scanning calorimetry from 298.15 K to 448.15 K under atmospheric pressure. No phase transition or other thermal anomaly was observed in the solid-phase region (298.15 K to 358.15 K) and liquid-phase region (403.15 K to 448.15 K). The basic properties and thermodynamic functions of the GIL, such as melting point, molar enthalpy and entropy of fusion, heat capacity, enthalpy H_T-$H_{298.15\,K}$, and entropy S_T-$S_{298.15\,K}$, were also determined from the experimental data. Thermal decomposition kinetics of $[PyC_6MPi][PF_6]_2$ were investigated by using non-isothermal thermogravimetric analysis in pure nitrogen atmosphere at various heating rates. Thermal decomposition data were, respectively, correlated with Friedman method, Ozawa-Flynn-Wall equation, and ASTM model. The activation energy (E) and pre-exponential factor (logA) values were obtained by using the above three methods.

Keywords: Gemini Gemini Ionic Liquid, Synthesis, Thermodynamic Properties, Heat Capacity, Thermal Decomposition

INTRODUCTION

Room-temperature ionic liquids (RTILs) have elicited increasing attention over the past few decades [1-3]. Gemini ionic liquids (GILs), a new type of ionic liquids consisting of two head groups combined with a spacer and two anions, have been recently reported [4-8]. GILs exhibit superior physicochemical properties in terms of volatility and thermal and chemical stability compared with traditional monocationic ionic liquids [9-11]. Given their tunability, GILs are more suitable for chemical and engineering applications in which ordinary RTILs fail, such as high-temperature organic synthesis [12-14], chromatography stationary phases [15,16], and potential electrolyte additives [17].

Recent research has reported the preparation and characterization of various symmetrical GILs in terms of their fascinating physicochemical properties [5]. The physicochemical properties of imidazolium-based symmetrical GILs were compared with those of monocationic ionic liquids containing various anions, and the unique and common features of these GILs were identified [18]. The lack of investigation on asymmetrical GILs is relatively self-evident for this class of ionic liquids compared with traditional monocationic ionic liquids [19]. Hence, the basic and thermodynamic properties of asymmetrical GILs, such as melting temperature T_m, heat capacity $C_{p,m}$, thermal decomposition temperature T_d, and enthalpy and entropy of phase transitions, should be determined. These data are important for any process involving asymmetrical GILs at an industrial scale, as well as to understand the applications of GILs in the academe and industry [20-25]. The basic and thermodynamic properties can be measured by differential scanning calorimetry (DSC) and thermogravimetric analysis (TGA).

In the current work, a novel asymmetrical GIL, [1-(1-pyridinium-yl-hexyl)-6-methylpiperidinium] dihexafluorophosphate ($[PyC_6MPi][PF_6]_2$), combined with pyridine and 1-methylpiperidine by 1,6-dibromohexane, was synthesized and characterized by ^1H NMR and IR. The heat capacity ($C_{p,m}$) of the GIL was measured by DSC from 298.15 K to 448.15 K under atmospheric pressure. The basic properties and thermodynamic functions of the GIL were determined from the experimental data. The thermal stability and decomposition process were investigated by non-isothermal TGA in pure nitrogen atmosphere at different heating rates. The thermal decomposition kinetic parameters were determined by using the Friedman, Ozawa-Flynn-Wall, and ASTM methods. The values of activation energy (E), pre-exponential factor (logA), and probable kinetic model of the thermal decomposition process were correspondingly obtained.

EXPERIMENTAL

1. Materials

The following reagents were used directly without further purification: 1,6-dibromohexane (Aladdin, 0.98), pyridine (Aladdin, 0.98), 1-methylpiperidine (Aladdin, 0.98), potassium hexafluorophosphate (Aladdin, 0.98), methanol (Aladdin, 0.98), and ethyl ace-

†To whom correspondence should be addressed.
E-mail: yangxz@zzuli.edu.cn, xuzhao5378@sina.com, wangjun8828@sina.com

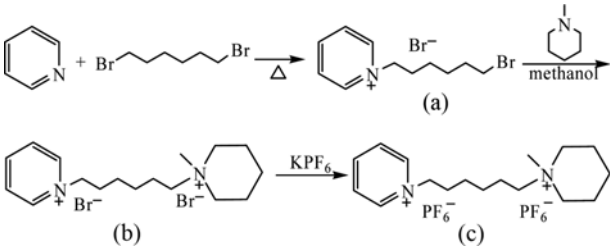

Scheme 1. Synthesis routes of asymmetrical dicationic ionic liquid ($[PyC_6MPi][PF_6]_2$).

tate (Aladdin, 0.98). All reagents are stable and stored under inert atmosphere.

2. Procedures

2-1. Synthesis and Characterization of $[PyC_6MPi][PF_6]_2$

Asymmetrical GIL $[PyC_6MPi][PF_6]_2$ was prepared in accordance with Scheme 1, and its purity was measured to be >0.99 in mass fraction by high-performance liquid chromatography (type Waters 600E, Waters Co.). The prepared asymmetrical GIL was stored under inert atmosphere. The procedure for the synthesis of 1-(6-bromohexyl) pridinium bromide (Compound a) was performed as follows: 1,6-dibromohexane (0.25 mol) was magnetically stirred in a flask at 50 °C followed by the dropwise addition of pyridine (0.05 mol); the mixture was reacted for 15 h and then filtered. The residue was rinsed thrice with ethyl acetate (20 mL) and dried in vacuo to yield a waxy-like solid; the total yield was 0.85 with 0.99 purity. [1-(1-pyridinium-yl-propyl)-6-methylpiperidinium] dibromide (Compound b) was prepared through the following steps: Compound a (0.05 mol) was mixed with N-methylpiperidine (0.055 mol) in methanol (dissolved Compound a as well) and stirred for 10 h at 60 °C, and then methanol was removed by evaporation. The residue was washed thrice with ethyl acetate and dried in vacuo at 60 °C for 12 h to obtain a white solid product (Compound b); the total yield was 0.95 with 0.99 purity. Compound c was synthesized through an anion exchange procedure, and the yield of $[PyC_6MPi][PF_6]_2$ was >0.90.

The obtained ionic liquid $[PyC_6MPi][PF_6]_2$ was identified by using ^{1}H NMR (Bruker Avance 400 spectrometer) and IR (Tensor-27 FT-IR Spectrometer). ^{1}H NMR (400 MHz, CD_2Cl_2) δ(ppm): δ 1.36 to 2.00 (m, 14H), δ 2.95 (d, 3H), δ 3.24 (t, 6H), δ 4.57 (t, 2H), δ 8.02 (t, 2H), δ 8.47 (m, 1H), δ 8.77 (t, 2H). IR (KBr): 3030, 2940, 1490, and 685 cm^{-1}.

2-2. Measurement of Heat Capacity

DSC is probably the most common method used to determine the heat capacity of ionic liquids. The heat capacity ($C_{p,m}$) of the GIL in this study was measured by DSC (DSC, Q100, TA Instruments). To verify the reliability of the DSC results, the molar heat capacities of synthetic sapphire (α-Al_2O_3) were measured. The deviations of the results from the recommended values by NIST 27 were within ±0.1% in the temperature range from 293.15 K to 453.15 K. The DSC conditions were described as follows: sample mass, ~10.0 mg; temperature range, 298.15 K to 448.15 K; and heating rate, 10 $K \cdot min^{-1}$.

2-3. Thermal Stability

Thermal stability and kinetics were determined by using a thermogravimetric analyzer (Netzsch STA 449C). The experiment conditions were determined as follows: sample mass, ~5.0 mg; heating rates: 5, 10, 15, 20, and 25 $K \cdot min^{-1}$; temperature range, 273.15 K to 1073.15 K; and highly pure nitrogen, 50 $mL \cdot min^{-1}$.

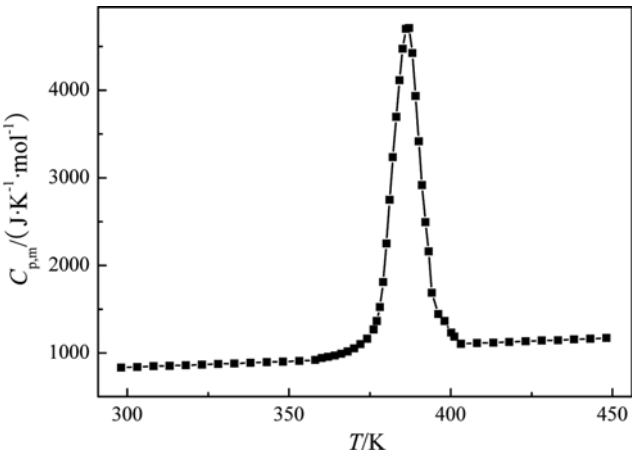

Fig. 1. The $C_{p,m}$ curve of ionic liquid $[PyC_6MPi]$ $[PF_6]_2$.

RESULTS AND DISCUSSION

1. Heat Capacity and Relative Thermodynamic Functions

The heat capacity curve of $[PyC_6MPi][PF_6]_2$ is shown in Fig. 1. As can be seen 1, the melting peak was relatively wide for the reason that the ionic liquid did not always convert directly into liquid during the phase-change process, which covered multiple phase-transition points: glass transition temperature and cooling point [26]. In a certain temperature range, ionic liquid exhibits tautomerism of mesomorphic phase leading to wide melting peaks. No phase transition or other thermal anomaly was observed in the solid range from 298.15 K to 358.15 K and liquid range from 403.15 K to 448.15 K for ionic liquid $[PyC_6MPi][PF_6]_2$. The melting point (T_m), phase transition enthalpy ($\Delta_{fus}H_m$), and phase transition entropy ($\Delta_{fus}S_m$) can be obtained from the curve. The $\Delta_{fus}H_m$ is the integral of the melting peak and $\Delta_{fus}S_m=\Delta_{fus}H_m/T_m$, which can be seen in Table 1.

The heat capacity of $[PyC_6MPi][PF_6]_2$ at various temperatures can be determined from the curve, and the data within the solid-phase region and liquid-phase region were correspondingly correlated with the following polynomial equation. The regression results are listed in Table 2.

$$C_{p,m}/(J \cdot mol^{-1} \cdot K^{-1}) = B_0 + B_1(T/K) + B_2(T/K)^2 \quad (1)$$

where T is the thermodynamic temperature (K), $C_{p,m}$ is the molar heat capacity ($J \cdot mol^{-1} \cdot K^{-1}$), and B_0-B_2 are the dimensionless equation constants.

Table 1. Basic properties of the gemini ionic liquid $[PyC_6MPi][PF_6]_2$

Ionic liquid	Basic properties		
	T_m/K	$\Delta_{fus}H_m$/($kJ \cdot mol^{-1}$)	$\Delta_{fus}S_m$/($J \cdot mol^{-1} \cdot K^{-1}$)
$[PyC_6MPi][PF_6]_2$	386.71	28.19	72.90

Table 2. The parameters of Eq. (1)

Ionic liquid	Solid phase region				Liquid phase region			
	B_0	B_1	B_2	R^2	B_0	B_1	B_2	R^2
$[PyC_6MPi][PF_6]_2$	833.8102	−1.1546	0.00388	0.9989	1339.4666	−2.4297	0.00458	0.9997

R^2: coefficient of determination

Table 3. The thermodynamic functions of $[PyC_6MPi][PF_6]_2$ obtained form heat capacity curve

Solid phase region				Liquid phase region			
T/K	$C_{p,m}$/ ($J\cdot mol^{-1}\cdot K^{-1}$)	H_T-$H_{298.15\,K}$/ ($kJ\cdot mol^{-1}$)	S_T-$S_{298.15\,K}$/ ($J\cdot mol^{-1}\cdot K^{-1}$)	T/K	$C_{p,m}$/ ($J\cdot mol^{-1}\cdot K^{-1}$)	H_T-$H_{298.15\,K}$/ ($kJ\cdot mol^{-1}$)	S_T-$S_{298.15\,K}$/ ($J\cdot mol^{-1}\cdot K^{-1}$)
298.15	833.32	0.00	0.00	403.15	1104.72	76.42	163.49
303.15	840.06	4.15	8.14	408.15	1111.03	83.09	167.91
308.15	847.85	8.28	16.16	413.15	1117.36	89.69	172.24
313.15	853.61	12.38	24.05	418.15	1124.32	96.24	176.49
318.15	859.46	16.46	31.82	423.15	1132.31	102.74	180.67
323.15	866.17	20.50	39.49	428.15	1139.65	109.17	184.77
328.15	873.01	24.53	47.05	433.15	1146.38	115.55	188.8
333.15	879.68	28.53	54.52	438.15	1153.96	121.88	192.77
338.15	886.17	32.51	61.89	443.15	1162.47	128.15	196.68
343.15	894.04	36.47	69.18	448.15	1171.03	134.38	200.53
348.15	901.53	40.41	76.39				
353.15	909.15	44.33	83.53				
358.15	919.72	48.23	90.59				

The thermodynamic functions relative to the standard reference temperature 298.15 K, such as enthapy H_T-$H_{298.15\,K}$ and entropy S_T-$S_{298.15\,K}$, were derived (Table 3) from the heat capacity data based on the following expressions:

Before the melting point,

$$H_T\text{-}H_{298.15\,K}=\int_{298.15\,K}^{T} C_{p,m}(s)dT \quad (2)$$

$$S_T\text{-}S_{298.15\,K}=\int_{298.15\,K}^{T} C_{p,m}(s)T^{-1}dT \quad (3)$$

After the melting point,

$$H_T\text{-}H_{298.15\,K}=\int_{298.15\,K}^{T_{f_1}} C_{p,m}(s)dT+\Delta_{fus}H_m+\int_{T_{f_2}}^{T} C_{p,m}(l)dT \quad (4)$$

$$S_T\text{-}S_{298.15\,K}=\int_{298.15\,K}^{T_{f_1}} C_{p,m}(s)T^{-1}dT + \Delta_{fus}H_m T_m^{-1}+\int_{T_{f_2}}^{T} C_{p,m}(l)T^{-1}dT \quad (5)$$

where T_1 is the initial fusion temperature (K), and T_2 is the final fusion temperature (K).

2. Thermal Stability

The TG curves of $[PyC_6MPi][PF_6]_2$ at various heating rates are shown in Fig. 2. As the heating rate increased, the onset decomposition temperatures (T_{onset}) laterally shifted to higher temperatures. Table 4 shows T_{onset} and the temperatures at the maximum rate of weight loss (T_{max}) at various heating rates from 5 K·min^{-1} to 25 K·min^{-1}. The T_{onset} and T_{max} of this type of dicationic ionic liquid were higher than those of traditional monocationic ionic liquids [27], proving that GILs demonstrate superior thermal stability. The lateral shift to higher temperatures for the maximum region of mass loss has been reported elsewhere [28]. The TG curves of $[PyC_6MPi]$ $[PF_6]_2$ at different heating rates showed that the ionic liquid presented only one-step thermal decomposition. As shown in Fig. 2 and Table 4, the total weight loss of $[PyC_6MPi][PF_6]_2$ during the decomposition processes slightly increased with increasing heating rates.

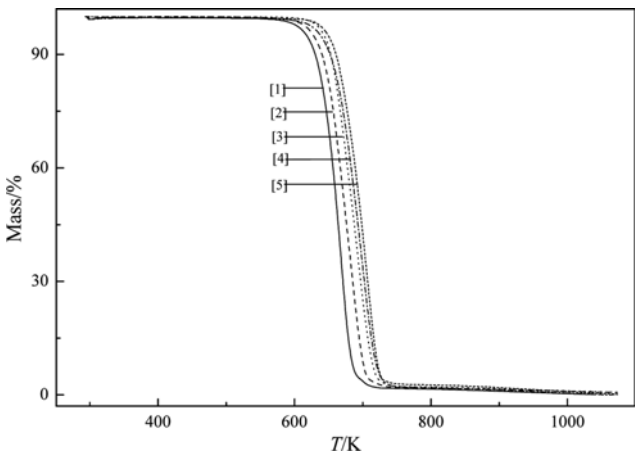

Fig. 2. The TG curves for decomposition of $[PyC_6MPi][PF_6]_2$ at different heating rates. (in K·min^{-1}): [1] 5, [2] 10, [3] 15, [4] 20, and [5] 25.

3. Decomposition Kinetics Analysis

In iso-conversional method, the degree of conversion α can be

Table 4. Characteristic temperatures in TG curves of $[PyC_6MPi][PF_6]_2$ at different heating rates

Heating rate/(K·min^{-1})	T_{onset}/K	T_{max}/K
5	632.35	671.65
10	643.49	685.95
15	651.53	695.25
20	658.26	700.85
25	666.67	707.45

explicitly assigned to each point of the reaction curves [24]. Three methods, ASTM, Friedman, and Ozawa-Flynn-Wall methods, were employed to determine the kinetic parameters of GIL thermal decomposition without knowing its decomposition mechanism.

3-1. ASTM Method

The ASTM method, which originated before the onset of the computer age, is usable only for one-step reactions. The standard equation can be expressed as follows [29-31]:

$$\ln\frac{\beta}{T_{max}^2}=\left(-\frac{E}{R}\right)\frac{1}{T_{max}}+\ln\frac{AR}{E} \quad (6)$$

where β is the heating rate (K·min^{-1}), E is the activation energy (kJ·mol^{-1}), R is the universal gas constant (8.314 J·mol^{-1}·K^{-1}), and T_{max} is the temperature at the maximum rate of weight loss (K).

The Kissinger plot shows a straight line with slope (−E/R). The $\ln(\beta/T^2_{max})$ is plotted over the $1/T_{max}$, where the obtained slope gives E. The pre-exponential factor (A) is obtained on the assumption of a single-step reaction.

3-2. Friedman Method

Friedman analysis is based on the following equation [25,32]:

$$\ln\left(\frac{d\alpha}{dt}\right)=\ln A-\frac{E}{RT}+\ln f(\alpha) \quad (7)$$

where $f(\alpha)$ is the reaction mechanism function. The plot of $\ln(d\alpha/dt)$ versus 1/T gives a group of straight lines, and E can be determined from the slopes.

3-3. Ozawa-Flynn-Wall Method

This method is an integral iso-conversion method reported by Ozawa [34] and Flynn-Wall [33] with the approach by Doyle (1962) for the exponential integral [33,34].

$$\log\beta=\lg\left[\frac{AE}{RG(\alpha)}\right]-2.315-\frac{0.4567E}{RT} \quad (8)$$

The plots of $\log\beta$ versus 1/T give a group of straight lines. The values of E at various conversions α can be, respectively, calculated from the slopes of the lines.

With these three methods, the values of E and log(A/s^{-1}) are shown in Table 5 and Fig. 3. The results of Friedman analysis showed that

Table 5. Thermal decomposition kinetic parameters obtained by Friedman, Ozawa-Flynn-Wall, and ASTM methods

α	Friedman		Ozawa-Flynn-Wall		ASTM	
	E/(kJ·mol^{-1})	log(A/s^{-1})	E/(kJ·mol^{-1})	log(A/s^{-1})	E/(kJ·mol^{-1})	log(A/s^{-1})
0.1	193.66	12.79	177.16	11.40	174.34±2.91	11.22
0.2	183.44	11.99	186.67	12.22		
0.3	171.16	11.02	185.28	12.12		
0.4	155.83	9.81	179.51	11.66		
0.5	143.40	8.86	172.30	11.08		
0.6	135.81	8.30	165.44	10.54		
0.7	131.18	7.99	159.18	10.06		
0.8	130.41	7.98	153.52	9.48		
0.9	149.64	9.40	149.31	9.32		
Average	154.95	9.79	169.82	10.88		

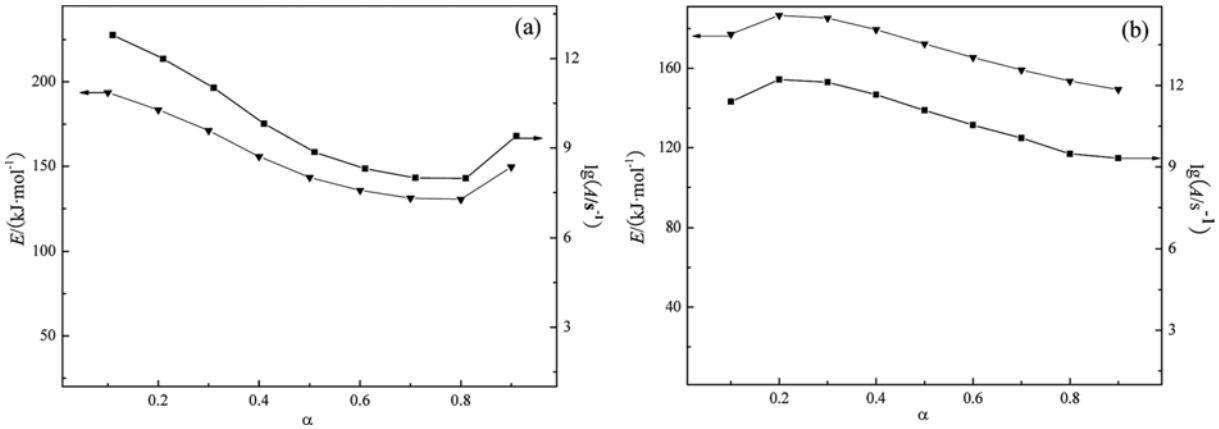

Fig. 3. The curves of E and A values in Friedman (a) analysis and Ozawa-Flynn-Wall method (b): ▼, E; ■, log(A/S^{-1}).

Table 6. Arrhenius parameters in multivariate non-linear-regression methods

Model	E/(kJ·mol^{-1})	log(A/s^{-1})	Correlation coefficient	n or lg$K_{cat.}$
C_1	163.72	10.08	0.9996	lg$K_{cat.}$=0.4127
F_n	181.83	11.75	0.9981	n=0.5233
F_1	196.44	14.31	0.9976	n=1
F_2	247.53	17.64	0.9891	n=2

the values of E were between 154.95 and 193.66 kJ·mol^{-1}, and the values of log(A/s^{-1}) values were in the range from 9.40 to 12.79, which decreased with an increase in the conversion (α) of [PyC_6MPi][PF_6]$_2$. The results from Ozawa-Flynn-Wall method showed that the activation energy values were between 169.82 and 177.16 kJ·mol^{-1}, and the log(A/s^{-1}) values were between 10.88 and 11.40, which were the same findings with the Friedman method. The activation energy obtained by the ASTM method was 174.34±2.91 kJ·mol^{-1}, and the corresponding average logarithmic pre-exponential factor was 11.22. The activation energy values and the pre-exponential factors calculated by the three methods were basically the same.

The probable kinetic model of thermal decomposition process can be determined by using the multiple linear regression method. In this study, Netzsch TA4 thermokinetics was used to estimate the kinetic parameters of mechanism function. On the basis of the correlation coefficient and single-step reaction observations, the mathematical models were obtained (Table 6). The C_1 model corresponds to the first-order reaction with autocatalysis, and the mechanism function f(α) is (1−α) (1+$K_{cat.}$ α), whereas the F_n model corresponds to nth-order reaction, and the f(α) in F_n is $(1-\alpha)^n$. As indicated in Table 6, the C_1 model is the most feasible model with the correlation coefficient of 0.9996. In addition, the corresponding E and log(A/s^{-1}) were, respectively, 163.72 kJ·mol^{-1} and 10.08, which were very similar to those from the Friedman and ASTM methods.

CONCLUSION

A novel asymmetrical gemini salt [PyC_6MPi][PF_6]$_2$ was synthesized and characterized. Its basic properties, such as melting point, phase transition enthalpy, phase transition entropy, and molar heat capacity, were measured by using DSC from 298.15 K to 448.15 K. The molar heat capacities of [PyC_6MPi][PF_6]$_2$ were fitted to polynomials: in solid-phase region, $C_{p,m}$/(J·mol^{-1}·K^{-1})=833.8102−1.1546 (T/K)+0.00388 (T/K)^2; and in liquid-phase region, $C_{p,m}$/(J·mol^{-1}·K^{-1})=1339.4666−2.4297 (T/K)+0.00458 (T/K)^2. Additionally, the thermodynamic functions relative to the standard reference temperature 298.15 K were determined. Thermal decomposition kinetics and mechanism function of [PyC_6MPi][PF_6]$_2$ were investigated by using TGA in pure nitrogen atmosphere. The average activation E, pre-exponential factor log(A/s^{-1}), and mechanism function f(α) were obtained by using three methods.

ACKNOWLEDGEMENTS

This work is financially supported by the National Natural Science Foundation of China (No. 21176228), Science and Technology Planning Project of Henan Province (No. 132102210188), Foundation for University Key Teacher of Henan Province (No. 2013GGJS-108), and Science and Technology Research Projects of Zhengzhou City (No. 141PQYJS555).

SYMBOLS

T_m : melting point
$C_{p,m}$: molar heat capacity
T_d : thermal decomposition temperature
T_{onset} : onset decomposition temperature
T_{max} : temperature at maximum mass loss rate
B_0-B_2 : dimensionless equation constants
T : thermodynamic temperature
T_1 : initial fusion temperature
T_2 : final fusion temperature
E : activation energy
A : pre-exponential factor
R : universal gas constant: 8.314 J·mol^{-1}·K^{-1}
f(α) : reaction mechanism function
G(α) : integral mechanism function
$K_{cat.}$: rate constant
n : reaction order
$S_{298.15\,K}$: entropy at 298.15 K
S_T : entropy at T

Greek Letters

$\Delta_{fus}H_m$: phase transition enthalpy
$\Delta_{fus}S_m$: phase transition entropy
β : heating rate
α : conversion
δ : chemical shift

Abbreviations

GIL : gemini ionic liquid
[PyC_6MPi][PF_6]$_2$: [1-(1-pyridinium-yl-hexyl)-6-methylpiperidinium] dihexafluorophosphate
NMR : nuclear magnetic resonance
IR : infrared spectroscopy
DSC : differential scanning calorimetry
TG : thermogravimetry
TGA : thermogravimetric analysis
ASTM : American society for testing and materials

REFERENCES

1. R. D. Rogers and K. R. Seddon, *Science*, **302**, 792 (2003).
2. L. Tang, G. Q. Luo, L. H. Kang, M. Y. Zhu and B. Dai, *Korean J. Chem. Eng.*, **30**, 314 (2013).
3. J. E. Kim, J. W. Kang and J. S. Lim, *Korean J. Chem. Eng.*, **32**, 1678 (2015).
4. X. X. Han and D. W. Armstrong, *Org. Lett.*, **7**, 4205 (2005).
5. J. L. Anderson, R. Ding, A. Ellern and D. W. Armstrong, *J. Am. Chem. Soc.*, **127**, 593 (2005).
6. M. Claros, H. R. Galleguillos, I. Brito and T. A. Graber, *J. Chem.*

Eng. Data, **57**, 2147 (2012).
7. X. J. Li, D. W. Bruce and J. M. Shreeve, *J. Mater. Chem.*, **19**, 8232 (2009).
8. K. C. Lethesh, K. V. Hecke, L. V. Meervelt, P. Nockemann, B. Kirchner, S. Zahn, T. N. Parac-Vogt, W. Dehaen and K. Binnemans, *J. Phys. Chem. B*, **115**, 8424 (2011).
9. Y. Yoshida, O. Baba, C. Larriba and G. Saito, *J. Phys. Chem. B*, **111**, 12204 (2007).
10. R. L. Gardas and J. A. P. Coutinho, *Ind. Eng. Chem. Res.*, **47**, 5751 (2008).
11. T. K. Carlisle, J. E. Bara and D. L. Gin, *Ind. Eng. Chem. Res.*, **47**, 7005 (2008).
12. J. H. Liang, X. Q. Ren, J. T. Wang, M. Jiang and Z. J. Li, *J. Fuel Chem. Technol.*, **38**, 275 (2010).
13. H. Z. Zhi, C. X. Lu, Q. Zhang and J. J. Luo, *Chem. Soc. Chem. Commun.*, **20**, 2878 (2009).
14. N. S. Gary and S. J. David, *Green Chem.*, **9**, 1044 (2007).
15. T. Payagala, Y. Zhang, E. Wanigasekara, K. Huang, Z. S. Breitbach, P. S. Sharma, L. M. Sidisky and D. W. Armstrong, *J. Anal. Chem.*, **81**, 160 (2009).
16. J. L. Anderson and D. W. Armstrong, *J. Anal. Chem.*, **77**, 6453 (2005).
17. Z. X. Zhang, H. Y. Zhou, L.Yang, K. Tachibana, K. Kamijima and J. Xu, *Electrochim. Acta*, **53**, 4833 (2008).
18. H. Shirota, T. Mandai, H. Fukazawa and T. Kato, *J. Chem. Eng. Data*, **56**, 2453 (2011).
19. T. Payagala, J. M. Huang, Z. S. Breitbach, P. S. Sharma and D. W. Armstrong, *J. Chem. Mater.*, **19**, 5848 (2007).
20. J. Wang, S. D. Wu and X. Z. Yang, *J. Chem. Eng. Data*, **55**, 3942 (2010).
21. J. O. Valderrama, A. Toro and R. E. Rojas, *J. Chem. Thermodyn.*, **43**, 1068 (2011).
22. A. F. Ferreira, P. N. Simoes and A. G. M. Ferreira, *J. Chem. Thermodyn.*, **45**, 16 (2012).
23. H. C. Hua, A. N. Soriano, R. B. Leron and M. H. Li, *Thermochim. Acta*, **519**, 44 (2011).
24. A. Chowdhury and S. T. Thynell, *Propell. Explos. Pyrot.*, **35**, 572 (2010).
25. R. Liang, M. R. Yang and X. P. Xuan, *Chin. J. Chem. Eng.*, **18**, 736 (2010).
26. J. R. Opfermann, E. Kaisersberger and H. J. Flammersheim, *Thermochim. Acta*, **391**, 119 (2012).
27. F. Heym, W. Korth, J. Thiessen, C. Kern and A. Jess, *Chem. Ing. Technol.*, **87**, 791 (2015).
28. X. J. Du, X. D. Li, M. S. Zou, R. J. Yang, S. P. Pang and Y. C. Li, *Thermochim. Acta*, **570**, 59 (2013).
29. J. Pitawala, A. Matic, A. Martinelli, P. Jacobsson, V. Koch and F. Croce, *J. Phys. Chem. B*, **113**, 10607 (2009).
30. H. E. Kissinger, *Anal. Chem.*, **29**, 1702 (1957).
31. E. S. Sashina, D. A. Kashirskii, G. Janowska and M. Zaborski, *Thermochim. Acta*, **568**, 185 (2013).
32. H. J. Friedman, *J. Polym. Sci., Part C: Polym. Symp.*, **6**, 183 (1964).
33. J. H. Flynn and L. A. Wall, *J. Polym. Sci. Part B: Polym. Lett.*, **4**, 32 (1966).
34. T. Ozawa, *Bull. Chem. Soc. Jpn.*, **38**, 1881 (1965).